

## Research Article

# Heat and Mass Transfer Analysis of Nanofluid Flow Based on Cu, Al<sub>2</sub>O<sub>3</sub>, and TiO<sub>2</sub> over a Moving Rotating Plate and Impact of Various Nanoparticle Shapes

W. Abbas <sup>1</sup> and M. M. Magdy<sup>2</sup>

<sup>1</sup>Basic and Applied Science Department, College of Engineering and Technology,  
Arab Academy for Science, Technology and Maritime Transport, Cairo, Egypt

<sup>2</sup>Maintenance and Operation Department, Safety Aviation Sector, Cairo Airport, Cairo, Egypt

Correspondence should be addressed to W. Abbas; wael\_abass@aast.edu

Received 3 January 2020; Revised 28 February 2020; Accepted 4 March 2020; Published 7 May 2020

Academic Editor: Mariano Torrisi

Copyright © 2020 W. Abbas and M. M. Magdy. This is an open access article distributed under the Creative Commons Attribution License, which permits unrestricted use, distribution, and reproduction in any medium, provided the original work is properly cited.

The study of rotating nanofluid flows has a vital role in several applications such as in food processing, rotating machinery, cooling systems, and chemical fluid. The aims of the present work are to improve the thermophysical properties of convective flow and heat transfer for unsteady nanofluid past a moving rotating plate in the presence of ohmic, viscous dissipations, Brownian, and thermophoresis diffusion. The system is strained under the effect of strong magnetic field, and then the Hall current is considered. For this investigation, three different types of the nanoparticles Cu (copper), Al<sub>2</sub>O<sub>3</sub> (aluminium oxide), and TiO<sub>2</sub> (titanium dioxide) with various shapes (spherical, cylindrical, and brick) are considered, and water is used as a base nanofluid. The system governing equations are solved semianalytically using homotopy perturbation technique. In order to validate the present work, different comparisons are made under some special cases with previously published results and found an excellent agreement. It is observed that the shape of nanoparticles plays a substantial role to significantly determine the flow behaviour. Also, it can be found that the use of the cylindrical nanoparticle shape has better improvement for heat transfer rate compared with the other nanoparticle shapes.

## 1. Introduction

In recent years, investigation of nanofluid flow has gained considerable interest by the researchers owing to increase in the implementations in different fields of technology, science, biomechanics, chemical, and nuclear industries. Nanofluid can be applied to engineering problems such as solar energy collection, heat exchangers, and engine cooling [1]. The term of nanofluids means the addition of small quantity of nanometer-sized particles nominally less than 100 nm into base fluids like oil, water, biofluids, ethylene, and lubricants. This term was first introduced by Choi [2]; he added small nanoparticles in a base fluid to increase the thermal conductivity. Eastmann et al. [3] discussed the thermal conductivity in ethylene glycol nanofluid-based copper nanoparticles. Since then, the growth of nanofluid mathematical modelling advances by demonstrating the characteristics of thermophoresis and Brownian diffusion.

Chamkha et al. [4] studied the thermal radiation effect on nanofluid boundary layer flow past a vertical cone. Time-dependent viscosity effect on free convection heat transfer of magnetohydrodynamic nanofluid was investigated by Sheikholeslami et al. [5]. Hayat et al. [1] investigated the flow with heat and mass transfer characteristics in magnetohydrodynamic (MHD) squeezing flow between two surfaces. The effect of Joule heating and Hall current on nanofluid flow along a vertical cone with heat and mass transfer was investigated by Abbas and Sayed [6]. Mahanthesh et al. [7] analyzed the effect of the novel exponential space-dependent heat source on magnetohydrodynamic nanofluid flow past a stretchable rotating disk with cross-diffusion and the convective condition. Later, many researchers have been engaged in recent developments on nanofluids [8–11].

Study of convective heat transfer and flow through magnetohydrodynamic nanofluid in the recent years has

received significant attraction by many researchers for their useful applications in both engineering and sciences such as reactors, cooling or heating processes, and solar energy. Shehzad et al. [12] studied the convective heat transfer effects of nanofluid flow on a wavy channel with Brownian and thermophoresis diffusion effect. Heat transfer of a nanofluid over a stretching sheet with considering the effects of temperature jump, slip velocity, and radiation was investigated by Shen et al. [13]. Jahan et al. [14] reported the nanofluid flow with stability and regression analysis of a permeable stretching sheet over the heated surface. In other studies, the convective heat transfer through nanofluid bounded by a moving rotating frame is investigated due to the increase in engineering and technological process applications. Hamad and Pop [15] studied heat transfer of unsteady nanofluid flow for a moving oscillatory plate with constant heat source. Nanofluid flow through two plates with rotating system in presence of magnetic field was reported by Sheikholeslami and Ganji [16]. Hussain et al. [17] presented the analytical solution of unsteady flow past a moving rotating plate considering the effects of Hall current and chemical reaction. Many investigators studied the thermocapillary convective with heat transfer on the fluid/nanofluid flow field under different categories and conditions [18–21].

The thermal radiation effect has attracted much attention for researchers for its enormous area of scientific and engineering applications such as electric power, food, solar cell panels, and medical industry [22]. Mahanthesh et al. [23] presented effects of nonlinear thermal radiation and suspended nanoparticles on mixed convection boundary layer nanofluid flow past a melting vertical surface. Kumar et al. [24] studied thermal analysis of bioconvection magneto-nanofluid flow containing gyrotactic microorganisms with second-order velocity slip and convective conditions. Raza et al. [25] presented the combined effects of thermal radiation and magnetic field of molybdenum disulfide nanofluid on a channel with shape effects.

Based on published literature, it is observed that the motion of nanofluid flow through a moving rotating plate has a significant potential role in several applications such as food processing, polymer processing, rotating machinery, cooling of metallic electronic component surfaces, and chemical fluid. Therefore, the objective of the present study is to investigate the effects of the nanoparticle shape, Brownian, and thermophoresis diffusion on the motion of MHD unsteady nanofluid flow

through past a moving rotating plate in the presence of ohmic, viscous dissipations, and thermal radiation. Three different types of the nanoparticles are considered. These types are copper, aluminium oxide, and titanium dioxide with various shapes (spherical, cylindrical, and brick), and water is used as a base nanofluid. The problem is formulated and solved semi-analytical using homotopy perturbation technique. Physical parameters are displayed and analyzed, and pertinent results are discussed in detail using graphs. Different comparisons are made under some special cases with previously published results which are conducted to validate the current results and prove efficiency of the methodology.

## 2. Mathematical Model and Formulation

**2.1. Problem Description.** Consider unsteady MHD nanofluid flow of ambient temperature  $T_\infty$  and concentration  $C_\infty$  with heat and mass transfer through the porous medium past a moving flat plate in a rotating frame. The coordinate system  $(x, y, z)$  is selected in such a way that  $x$  – axis is taken along the plate,  $z$  – axis is perpendicular to it, and  $y$  – axis is normal to the  $(xz)$  plane. The physical model is described in Figure 1. Three different kinds of nanoparticles, Cu (copper),  $Al_2O_3$  (aluminium oxide), and  $TiO_2$  (titanium dioxide), with water used as a base nanofluid are considered. The fluid and nanoparticles are assumed to have no slip between them, and both are in thermal equilibrium. Table 1 clearly lists the thermophysical properties of the base fluid and different nanoparticles [26, 27]. In this work, there are three shapes of nanoparticles which are spherical, cylindrical, and brick employed into account. Also, the model is assumed rotating about  $z$  – axis with constant angular velocity  $\Omega$ . The fluid is permeated by applied time-dependent magnetic field which takes the form  $B(t) = G(e^{-\alpha t})$  which is taken to be acting along the positive  $z$ -direction, where  $G$  and  $\alpha$  are constants. It is assumed that the magnetic Reynolds number is to be very small so that the induced magnetic field can be neglected, and there is no applied external electric field. It is also assumed that the frequency of electron-atom collision to be relatively high so that the Hall effect cannot be neglected.

**2.2. Governing Equations.** With above assumptions, the nanofluid flow is governed by conservations of continuity, momentum, energy, and concentration equations as

$$\begin{aligned}
 \nabla \cdot \mathbf{V} &= 0, \\
 \frac{\partial \mathbf{V}}{\partial t} + (\mathbf{V} \cdot \nabla) \mathbf{V} - \Omega \times \mathbf{V} &= \frac{1}{\rho_{nf}} \left[ \nabla(\mu \cdot \nabla \mathbf{V}) + \mathbf{J} \times B(t) + F_T + F_C + F_p \right], \\
 \frac{\partial T}{\partial t} + (\mathbf{V} \cdot \nabla) T &= \frac{1}{(\rho C p)_{nf}} \left[ \nabla(k_{nf} \cdot \nabla T) + \frac{\mathbf{J} \cdot \mathbf{J}}{\sigma_{nf}} + \frac{D_m k_T \rho_{nf}}{C_s} \nabla \cdot (\nabla C) \rho_s C p_s \left( D_B (\nabla T \cdot \nabla C) + \frac{D_T}{T_\infty} (\nabla T \cdot \nabla T) \right) \right. \\
 &\quad \left. + Q_0 (T - T_\infty) + \varphi - \nabla \cdot \mathbf{q}_r \right], \\
 \frac{\partial C}{\partial t} + (\mathbf{V} \cdot \nabla) C &= \nabla \cdot \left[ D \nabla C + \frac{D_T}{T_\infty} \nabla T \right] + k_c (C - C_\infty),
 \end{aligned} \tag{1}$$

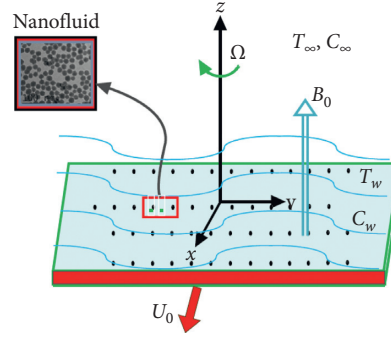


FIGURE 1: Physical model of the problem.

TABLE 1: Thermophysical properties [26, 27].

Thermophysical properties	Water H <sub>2</sub> O	Copper Cu	Aluminium oxide Al <sub>2</sub> O <sub>3</sub>	Titanium dioxide TiO <sub>2</sub>
$C_p$ (J/kgK)	4179.00	385.00	765.00	686.00
$\rho$ (kg/m <sup>3</sup> )	997.10	8933.00	3970.00	4250.00
$K$ (W/mK)	0.613	400.00	46.00	8.90
$\beta^* \times 10^{-5}$ (1/K)	21	1.67	0.63	1.05
$\sigma$ (S/m)	$5.50 \times 10^{-6}$	$1163.10 \times 10^7$	$131.70 \times 10^7$	$2.38 \times 10^6$

where  $\rho_{nf}$  is the nanofluid density,  $\mathbf{V}$  denotes the velocity vector which has the following components:  $\mathbf{V} = (u(z, t), v(z, t), w_0)$ ,  $\mu$  is the nanofluid viscosity,  $F_T$  is the thermal expansion term due to temperature difference,  $F_C$  denotes the thermal expansion term due to concentration difference,  $F_p$  is the porous medium term,  $C_p \rho_{nf}$  denotes the nanofluid specific heat at constant pressure,  $k_{nf}$  denotes the nanofluid thermal conductivity,  $\sigma_{nf}$  is the electric conductivity,  $D_m$  denotes the mass diffusivity,  $k_T$  is the thermal diffusivity,  $C_s$  denotes the susceptibility of concentration,  $\rho_s C_p$  denotes the nanoparticle heat capacity, and  $D_B$  and  $D_T$  denote the Brownian and thermophoresis coefficient, respectively.  $Q_0$  is the source constant, and  $\varphi$  is the viscous dissipation term.  $q_r$  is the radiative heat flux,  $T_m$  is the mean temperature, and  $k_c$  is the chemical reaction coefficient.  $J$  denotes the electric current density which is formulated by generalized Ohm's law including Hall current as [28–30]

$$J = \sigma_{nf} [V \times B - \xi (J \times B)], \quad (2)$$

where  $\xi$  is the Hall factor.

Furthermore, radiative heat flux is formulated by Rosseland approximation as

$$q_r = -\frac{4\sigma^*}{3\alpha^*} \frac{\partial T^4}{\partial z}. \quad (3)$$

$\sigma^*$  and  $\alpha^*$  denote the constant Stefan–Boltzman and mean absorption coefficient, respectively. Consider temperature differences are sufficiently small, and the term  $T^4$  can be expressed as a linear function into the Taylor series about  $T_\infty$ , and after neglecting higher-order terms, it yields

$$T^4 \cong 4T_\infty^3 T - 3T_\infty^4. \quad (4)$$

Under the assumptions made above, the governing equations are as follows:

$$\rho_{nf} \left( \frac{\partial u}{\partial t} + w_0 \frac{\partial u}{\partial z} + 2\Omega v \right) = \mu_{nf} \frac{\partial^2 u}{\partial z^2} - \frac{\sigma_{nf} B^2(t)}{1+m^2} (u + mv) - \frac{\mu_{nf}}{k_p} u + \rho_{nf} \beta_{T,nf}^* g (T - T_\infty) + \rho_{nf} \beta_{C,nf}^* g (C - C_\infty), \quad (5)$$

$$\rho_{nf} \left( \frac{\partial v}{\partial t} + w_0 \frac{\partial v}{\partial z} - 2\Omega u \right) = \mu_{nf} \frac{\partial^2 v}{\partial z^2} - \frac{\sigma_{nf} B^2(t)}{1+m^2} (v - mu) - \frac{\mu_{nf}}{k_p} v, \quad (6)$$

$$\begin{aligned} \rho_{nf} C_{p,nf} \left( \frac{\partial T}{\partial t} + w_0 \frac{\partial T}{\partial z} \right) &= k_{nf} \frac{\partial^2 T}{\partial z^2} + \mu_{nf} \left( \frac{\partial u}{\partial z} \right)^2 + \frac{\sigma_{nf} B^2(t)}{1+m^2} (u^2 + v^2) + Q(T - T_\infty) + \frac{D_m k_T \rho_{nf}}{C_s} \frac{\partial^2 C}{\partial z^2} \\ &\quad + \rho_s C_p \left[ D_B \frac{\partial C}{\partial z} \frac{\partial T}{\partial z} + \frac{D_T}{T_\infty} \left( \frac{\partial T}{\partial z} \right)^2 \right] - \frac{16\sigma^* T_\infty^3}{3\alpha^*} \frac{\partial^2 T}{\partial z^2}, \end{aligned} \quad (7)$$

$$\frac{\partial C}{\partial t} + w_0 \frac{\partial C}{\partial z} = D \frac{\partial^2 C}{\partial z^2} + k_c (C - C_\infty) + \frac{D_T}{T_\infty} \frac{\partial^2 T}{\partial z^2}, \quad (8)$$

where  $\beta_{Tnf}^*$  denotes the nanofluid thermal expansion coefficient due to temperature difference,  $\beta_{Cnf}^*$  denotes the nanofluid thermal expansion coefficient due to concentration difference, and  $m = \sigma_{nf}\xi B_0$  is the Hall parameter [31].

The boundary conditions are

$$\begin{aligned} t \leq 0: u &= 0, \\ w &= 0, \\ T &= T_\infty, \\ C &= C_\infty, \\ z &= 0, \\ t > 0: u &= U_0, \\ w &= 0, \\ T &= T_w, \\ C &= C_w \\ z &\longrightarrow \infty, \\ t > 0: u &\longrightarrow 0, \\ w &\longrightarrow 0, \\ T &\longrightarrow T_\infty, \\ C &\longrightarrow C_\infty. \end{aligned} \quad (9)$$

**2.3. Thermophysical Properties of Nanofluid.** The nanofluid thermophysical properties were calculated using the following forms [6, 26]:

Nanofluid effective dynamic viscosity, effective density, and heat capacity are given as

$$\begin{aligned} \mu_{nf} &= \frac{\mu_f}{(1-\phi)^{2.5}}, \\ J_1 &= \frac{\rho_f}{\rho_{nf}} = \frac{1}{(1-\phi) + \phi(\rho_s/\rho_f)}, \\ J_2 &= \frac{(\rho C p)_f}{(\rho C p)_{nf}} = \frac{1}{(1-\phi) + \phi((\rho C p)_s/(\rho C p)_f)}, \end{aligned} \quad (10)$$

where  $\phi$  denotes the nanofluid volume fraction. Subscripts  $f$ ,  $nf$ , and  $s$  denote the base fluid, nanofluid, and solid particle, respectively.

Also, nanofluid effective electric conductivity and effective thermal expansion coefficient are given as

$$\begin{aligned} J_3 &= \frac{\sigma_{nf}}{\sigma_f} = 1 + \frac{3((\sigma_s/\sigma_f) - 1)\phi}{((\sigma_s/\sigma_f) + 2) - ((\sigma_s/\sigma_f) - 1)\phi}, \\ J_4 &= \frac{(\rho\beta^*)_{nf}}{(\rho\beta^*)_f} = (1-\phi) + \phi \frac{(\rho\beta^*)_s}{(\rho\beta^*)_f}. \end{aligned} \quad (11)$$

Effective thermal conductivity and effect of nanoparticle shapes are considered by using the Hamilton and Crosser model as [26]

$$J_5 = \frac{k_{nf}}{k_f} = \frac{k_s + (n_p - 1)k_f - (n_p - 1)\phi(k_f - k_s)}{k_s + (n_p - 1)k_f + \phi(k_f - k_s)}, \quad (12)$$

where  $n_p$  indicates the empirical nanoparticle shape factor which is given by

$$n_p = \frac{3}{\Psi_s}. \quad (13)$$

Here,  $\Psi_s$  is the sphericity of the nanoparticles which is defined as the ratio of the surface area of a sphere to the area of the particle with a volume equal to that of a particle and has value 1 ( $n_p = 3$ ) for spherical-shaped nanoparticles and 0.5 ( $n_p = 6$ ) for spherical-shaped nanoparticles. The characteristics of shape factor  $n_p$  for various nanoparticle shapes have been displayed in Table 2 [32].

Introducing the following nondimensional variables,

$$\begin{aligned} (\hat{x}, \hat{y}, \hat{z}) &= \frac{(x, y, z)U_0}{\nu_f}, \\ \hat{t} &= \frac{U_0^2}{\nu_f} t, \\ \hat{u} &= \frac{u}{U_0}, \\ \hat{w} &= \frac{w}{U_0}, \\ \theta &= \frac{T - T_\infty}{T_w - T_\infty}, \\ \Gamma &= \frac{C - C_\infty}{C_w - C_\infty}. \end{aligned} \quad (14)$$

Governing equations (5)–(8) are reduced to nondimensional form after dropping the cap as

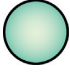

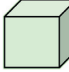
$$\begin{aligned} \frac{\partial u}{\partial t} + s \frac{\partial u}{\partial z} + Rv &= \frac{J_1}{(1-\phi)^{2.5}} \frac{\partial^2 u}{\partial z^2} - \frac{Ha^2 J_1 J_3}{1+m^2} (u+mv) \\ &+ G_r J_1 J_4 \theta + G_c J_1 J_4 \Gamma - \frac{MJ_1}{(1-\phi)^{2.5}} u, \end{aligned} \quad (15)$$

$$\begin{aligned} \frac{\partial v}{\partial t} + s \frac{\partial v}{\partial z} - Ru &= \frac{J_1}{(1-\phi)^{2.5}} \frac{\partial^2 v}{\partial z^2} - \frac{Ha^2 J_1 J_3}{1+m^2} (v-mu) \\ &- \frac{MJ_1}{(1-\phi)^{2.5}} v, \end{aligned} \quad (16)$$

$$\begin{aligned} \frac{\partial \theta}{\partial t} + s \frac{\partial \theta}{\partial z} &= \frac{1}{P_r} J_5 J_2 \frac{\partial^2 \theta}{\partial z^2} + \frac{Ha^2 E_c}{1+m^2} J_3 J_2 (u^2 + v^2) + Q_s J_2 \theta \\ &- Q_r J_2 \frac{\partial^2 \theta}{\partial z^2} + D_u J_2 \frac{\partial^2 \Gamma}{\partial z^2} + N_B J_2 \frac{\partial \theta}{\partial z} \frac{\partial \Gamma}{\partial z} + N_T J_2 \left( \frac{\partial \theta}{\partial z} \right)^2 \\ &+ \frac{E_c}{(1-\phi)^{2.5}} J_2 \left( \left( \frac{\partial u}{\partial z} \right)^2 + \left( \frac{\partial v}{\partial z} \right)^2 \right), \end{aligned} \quad (17)$$

$$\frac{\partial \Gamma}{\partial t} + s \frac{\partial \Gamma}{\partial z} = \frac{1}{S_c} \frac{\partial^2 \Gamma}{\partial z^2} + \gamma_c \Gamma + S_r \frac{\partial^2 \theta}{\partial z^2}, \quad (18)$$

TABLE 2: Shape factor for various nanoparticle shapes [32].

	Spherical	Cylindrical	Brick
Shapes of nanoparticles			
Shape factor ( $n_p$ )	3	6	3.7

where  $R = (2\Omega\nu_f)/U_0^2$  is the rotation parameter,  $Ha^2 = \mu_f B_0^2 \sigma_f / \rho_f^2 U_0^2$  is the Hartmann number squared,  $G_r = g\nu_f \beta_{Tf}^* (T_w - T_\infty) / U_0^3$  is the Grashof number,  $G_c = g\nu_f \beta_{Cf}^* (C_w - C_\infty) / U_0^3$  is the modified Grashof number,  $M = \mu_f^2 / U_0^2 k \rho_f^2$  is the porous medium parameter,  $P_r = C_{pf} \mu_f / k_f$  is the Prandtl number,  $E_c = U_0^2 / C_{pf} (T_w - T_\infty)$  is the Eckart number,  $Q_s = Q\nu_f / U_0^2 (\rho C_p)_f$  is the heat source parameter,  $Q_r = 16\sigma T_\infty^3 / 3\alpha^* \nu_f (\rho C_p)_f$  is the radiation parameter,  $D_u = (D_m k_T (C_w - C_\infty)) / (C_s C_{pf} \nu_f (T_w - T_\infty))$  is the Dufour number, Brownian parameter  $N_B = D_B \tau (C_w - C_\infty) / \nu_f$ ,  $N_T = D_T \tau (T_w - T_\infty) / \nu_f T_\infty$  denotes thermophoresis parameter, nanoparticles and base fluid heat capacity ratio is  $\tau = \rho_s C_{ps} / \rho_f C_{pf}$ ,  $S_c = \nu_f / D$  is the Schmidt number,  $\gamma_c = k_c \nu_f / U_0^2$  is the chemical reaction parameter, and  $S_r = D_T (T_w - T_\infty) / T_\infty (C_w - C_\infty)$  denotes the Soret number.

The boundary conditions reduce to

$$\begin{aligned}
 t = 0: u &= 0, \\
 w &= 0, \\
 \theta &\longrightarrow 0, \\
 \Gamma &\longrightarrow 0, \\
 z &= 0, \\
 t > 0: u &= 1, \\
 w &= 0, \\
 \theta &= 1, \\
 \Gamma &= 1, \\
 z &\longrightarrow \infty, \\
 t > 0: u &\longrightarrow 0, \\
 w &\longrightarrow 0, \\
 \theta &\longrightarrow 0, \\
 \Gamma &\longrightarrow 0.
 \end{aligned} \tag{19}$$

**2.4. Engineering Interest Physical Quantities.** For engineering interest, the local skin friction ( $C_f$ ), local Nusselt number ( $Nu_x$ ), and local Sherwood number ( $Sh_x$ ) are defined as [33–35]

$$\begin{aligned}
 C_f &= \frac{\tau_w}{\rho_f U_0^2}, \\
 Nu_x &= \frac{x q_w}{k_f (T_w - T_\infty)}, \\
 Sh_x &= \frac{x q_m}{D_B (T_w - T_\infty)},
 \end{aligned} \tag{20}$$

where  $\tau_w$ ,  $q_w$ , and  $q_m$  denote the wall shear stress and heat and mass fluxes, respectively, which are given by

$$\begin{aligned}
 \tau_w &= \mu_{nf} \left( \frac{\partial u}{\partial z} \right)_{z=0}, \\
 q_w &= -k_{nf} \left( \frac{\partial T}{\partial z} + q_r \right)_{z=0}, \\
 q_m &= -D_B \left( \frac{\partial C}{\partial z} \right)_{z=0}.
 \end{aligned} \tag{21}$$

By substituting equation (14) into equations (20) and (21),

$$Nu_x = -\frac{k_{nf}}{k_f} Re_x (1 + Q_r) \theta' (0), \tag{22}$$

where  $Re_x = U_0 x / \nu_f$  is the local Reynolds number.

### 3. Methodology

Here, the homotopy perturbation method that was first developed by He [36, 37] and improved by Wu and He [38] to solve governing equations (15)–(18) subject to boundary condition (19) is used. To illustrate the fundamental ideas of this method, we first consider the time-dependent differential equation as follows:

$$Y(\zeta(\lambda, t)) - f(\lambda, t) = 0, \quad \lambda \in \mathfrak{R}, \tag{23}$$

where  $Y$  is the operator,  $\zeta(\lambda, t)$  denotes the unknown function,  $f(\lambda, t)$  is a known function,  $\lambda$  are spatial variables,  $t$  denote temporal independent variables, and  $\mathfrak{R}$  is the domain.

The operator  $Y$  can be decomposed into the linear part  $L(\lambda, t)$ , and  $N(\lambda, t)$  is the remaining part. Therefore, equation (23) can be rewritten as

$$L(\lambda, t) + N(\lambda, t) - f(\lambda, t) = 0, \quad \lambda \in \mathfrak{R}. \tag{24}$$

Homotopy traditional technique constructs a homotopy function  $\Psi(\lambda, t; p)$  as follows:

$$\begin{aligned}
 H[\Psi(\lambda, t; p)] &= (1 - p)[L\Psi(\lambda, t; p) - L(f_0(\lambda, t))] \\
 &+ p[Y(\Psi(\lambda, t; p)) - f(\lambda, t)] = 0,
 \end{aligned} \tag{25}$$

where  $p \in [0, 1]$  is an embedding parameter and  $f_0(\lambda, t)$  is an initial guess approximation of equation (23) which satisfies boundary and initial condition.

Consequently, the solution of equation (23) is expressed as

$$\Psi((\lambda, t; p)) = \sum_{i=0}^n \Psi_i(\lambda, t) p^i. \tag{26}$$

Ideal approximation solution can be obtained when  $p = 1$  as

$$\zeta((\lambda, t)) = \sum_{i=0}^n \zeta_i(\lambda, t). \tag{27}$$

According to equation (24), the appropriate initial arbitrary guess approximation and linear operators for each equation are proposed as

$$\begin{aligned}
 u_0 &= y(1 + e^{-t}), \\
 v_0 &= y(1 + e^{-t}), \\
 \theta_0 &= y(1 - e^{-t}), \\
 \Gamma_0 &= y(1 - e^{-t}). \\
 L(u) &= \frac{\partial^2 u}{\partial z^2}, \\
 L(v) &= \frac{\partial^2 v}{\partial z^2}, \\
 L(\theta) &= \frac{\partial^2 \theta}{\partial z^2}, \\
 L(\Gamma) &= \frac{\partial^2 \Gamma}{\partial z^2}.
 \end{aligned} \tag{28}$$

Now, HPM constructed equations which satisfy equation (25) to governing nonlinear differential equations (15)–(18) as follows:

$$H(u; p) = p \left( \frac{J_1}{(1-\phi)^{2.5}} L(u) \right) + (1-p) \left( -\frac{\partial u}{\partial t} - s \frac{\partial u}{\partial z} - Rv - \frac{Ha^2 J_1 J_3}{1+m^2} (u + mv) + G_r J_1 J_4 \theta + G_c J_1 J_4 \Gamma - \frac{MJ_1}{(1-\phi)^{2.5}} u \right) = 0, \tag{29}$$

$$H(v; p) = p \left( \frac{J_1}{(1-\phi)^{2.5}} L(v) \right) + (1-p) \left( -\frac{\partial v}{\partial t} - s \frac{\partial v}{\partial z} - Ru - \frac{Ha^2 J_1 J_3}{1+m^2} (v - mu) - \frac{MJ_1}{(1-\phi)^{2.5}} v \right) = 0, \tag{30}$$

$$\begin{aligned}
 H(\theta; p) &= p \left( \left( \frac{1}{P_r} J_5 J_2 - Q_r J_2 \right) L(\theta) \right) + (1-p) \left( \frac{\partial \theta}{\partial t} + s \frac{\partial \theta}{\partial z} + \frac{Ha^2 E_c}{1+m^2} J_3 J_2 (u^2 + v^2) + Q_s J_2 \theta + D_u J_2 \frac{\partial^2 \Gamma}{\partial z^2} \right. \\
 &\quad \left. + N_B J_2 \frac{\partial \theta}{\partial z} \frac{\partial \Gamma}{\partial z} + N_T J_2 \left( \frac{\partial \theta}{\partial z} \right)^2 + \frac{E_c}{(1-\phi)^{2.5}} J_2 \left( \left( \frac{\partial u}{\partial z} \right)^2 + \left( \frac{\partial v}{\partial z} \right)^2 \right) \right) = 0,
 \end{aligned} \tag{31}$$

$$H(\Gamma; p) = p \left( \frac{1}{S_C} L(\Gamma) \right) + (1-p) \left( -\frac{\partial \Gamma}{\partial t} - s \frac{\partial \Gamma}{\partial z} + \gamma_c \Gamma + S_r \frac{\partial^2 \theta}{\partial z^2} \right) = 0. \tag{32}$$

And, assuming the solution of equations (29)–(32), it can be written in the following forms:

$$\begin{aligned}
 u(z, t) &= u_1(t)z + u_2(t)z^2 + u_3(t)z^3 + \dots, \\
 v(z, t) &= v_1(t)z + v_2(t)z^2 + v_3(t)z^3 + \dots, \\
 \theta(z, t) &= \theta_1(t)z + \theta_2(t)z^2 + \theta_3(t)z^3 + \dots,
 \end{aligned}$$

$$\Gamma(z, t) = \Gamma_1(t)z + \Gamma_2(t)z^2 + \Gamma_3(t)z^3 + \dots \tag{33}$$

Substituting equation (26) into equations (27)–(31) after some simplifications and rearranging depending on powers of  $p$ -terms and solved using conditions (19), the following approximations can be obtained:

$$\begin{aligned}
 u_1(t) &= \frac{15}{90J_1} e^{-\alpha t} (1-\phi)^{5/2} (MJ_1(1+e^{\alpha t}) + Ha^2 J_1 J_4 A_1 (1+e^{\alpha t}) + G_c J_1 J_3 (1-e^{\alpha t}) - \alpha(1-s)G_r J_1 J_2 (1-e^{\alpha t}) + R(1+e^{\alpha t})), \\
 u_2(t) &= \frac{32}{3J_1} e^{-\alpha t} (1-\phi)^{5/2} (MJ_1(1+e^{\alpha t}) + Ha^2 J_1 J_4 A_1 (1+e^{\alpha t}) + G_c J_1 J_3 (1-e^{\alpha t}) - \alpha(1+s) - G_r J_1 J_2 (1-e^{\alpha t}) + R(1+e^{\alpha t})), \\
 u_3(t) &= \frac{15}{90J_1} (1-\phi)^{5/2} (Ha^2 J_1 J_4 (1-m) - R - \alpha - e^{\alpha t}), \\
 v_1(t) &= \frac{15}{90} (1-\phi)^{5/2} \left( -e^{-\alpha t} (R + \alpha s) + Ha^2 J_4 J_1 \left( \frac{90}{15} e^{-\alpha t} + m^2 - m^3 + A_1 e^{-\alpha t} \right) \right), \\
 v_2(t) &= -\frac{32}{3} Ha^2 J_1 J_4 (1-\phi)^{5/2} + R(1-\phi)^{5/2} + Ha^2 J_1 J_4 m (1-\phi)^{5/2} + \frac{32}{3} \alpha e^{-\alpha t} (1-\phi)^{5/2} - \frac{32}{3} Ha^2 J_1 J_4 e^{-\alpha t} (1-\phi)^{5/2} \\
 &\quad + \frac{32}{3} Re^{-\alpha t} (1-\phi)^{5/2}, \\
 v_3(t) &= -MJ_1 (1-\phi)^{5/2} + Ha^2 J_4 m^3 e^{-\alpha t} (1-\phi)^{5/2} \frac{32}{3} - 0.125, \\
 \theta_1 &= -\frac{32P_r e^{-\alpha t} (\alpha + J_6 Q_r (1 - e^{\alpha t}))}{3J_5 J_6} + \frac{4P_r e^{-2\alpha t} (e^{\alpha t} - 1) (s e^{\alpha t} + D_N B J_6 (1 - e^{\alpha t}))}{J_5 J_6} - \frac{256E_c Ha^2 J_4 P_r e^{-2\alpha t} (m^2 + 1) (e^{\alpha t} + 1)^2}{3J_5} + \frac{1}{8}, \\
 \theta_2 &= \frac{P_r e^{-2\alpha t} (e^{\alpha t} - 1) (s e^{\alpha t} + D_N B J_6 (1 - e^{\alpha t}))}{2J_5 J_6}, \\
 \theta_3 &= \frac{P_r e^{-\alpha t} (\alpha + J_6 Q_r (1 - e^{\alpha t}))}{6J_5 J_6}, \\
 \Gamma_1(t) &= \frac{S_c e^{-\alpha t} (\alpha - \gamma_c (1 + e^{\alpha t}))}{6}, \\
 \Gamma_2(t) &= \frac{32S_c e^{-\alpha t} (\alpha - \gamma_c (1 + e^{\alpha t}))}{3} - 4S_c e^{-\alpha t} (Sr + s)(e^{\alpha t} - 1) - 0.125, \\
 \Gamma_3(t) &= \frac{S_c e^{-\alpha t} (Sr + s)(e^{\alpha t} - 1)}{2},
 \end{aligned} \tag{34}$$

where  $A_1 = m^3 + m^2 + m + 1$  and  $A_2 = -m^3 + m^2 - m$ .

### 4. Solution Validation

To check the accuracy and efficiency of the methodology, the current results are verified by comparing with previously published results in some special cases which are tabulated in Tables 3–5. The present results of different skin friction coefficient values  $C_f$  and Nusselt number  $Nu/Re_x$  for different values of nanoparticle volume fraction  $\phi$  and rotation parameter  $R$  are compared with those reported by Das [39] and Reddy et al. [40] with both nanoparticles Cu and  $Al_2O_3$  which are illustrated in Tables 3 and 4. The results obtained come with excellent agreement of previous studies.

Furthermore, the comparison for different values of the Sherwood number  $-Sh_x$  against time  $t$  and chemical reaction  $\gamma_c$  with obtained results by Hussain et al. [17] at  $\phi = 0.0$  is listed in Table 5. Also, it can be seen that the present obtained results are in an excellent agreement with the

previously published results. This proves the validity of the present work and shows how powerful the solution reached by homotopy perturbation technique.

### 5. Results and Discussion

The influence of various physical parameters such as nanoparticle volume fraction  $\phi$ , shape of nanoparticles  $n_p$ , Hall current  $m$ , Brownian  $N_B$ , thermophoretic  $N_T$ , and chemical reaction  $\gamma_c$  which are computed from the approximate solution reported in the previous section is displayed graphically and discussed. The graphical results are illustrated in Figures 2–11. The numerical results are performed by taking values of some constant parameters as  $s = 0.5$ ,  $M = 0.5$ ,  $P_r = 0.7$ ,  $E_c = 0.2$ ,  $G_c = 1$ ,  $G_r = 1$ ,  $S_c = 0.3$ ,  $D_u = 0.5$ ,  $G = 5$ , and  $S_r = 0.5$ .

Figures 2 and 3 display the effect of nanoparticle volume fraction parameter  $\phi$  on the fluid velocity  $u$  and temperature profiles  $\theta$  for either Cu – water,  $Al_2O_3$  – water,

TABLE 3: Result comparison for  $C_f$ .

$\phi$	$R$	$C_f$			$Al_2O_3$ -water		
		Present	Das [39]	Reddy et al. [40]	Present	Das [39]	
0.00	0.3	2.0355	2.0354	2.03542	2.0355	2.0354	
0.04		2.3158	2.3154	2.31535	0.5134	2.1831	
0.08		2.6111	2.6107	2.61068	2.1832	2.3384	
0.12		2.9120	2.9196	2.91953	2.5030	2.5020	
0.14	0.0	3.0792	3.0789	3.07891	1.0885	1.0872	
0.05		2.3790	2.3786	2.37862	2.2144	2.2143	
		0.5	2.4042	2.4040	2.40401	2.2333	2.2333
		1.5	2.5755	2.5755	2.57546	2.3669	2.3666
	2.5	2.8236	2.8235	2.8251	2.5697	2.5695	

TABLE 4: Result comparison for  $Nu_x/Re_x$ .

$\phi$	$R$	$Nu_x/Re_x$			$Al_2O_3$ -water	
		Present	Das [39]	Reddy et al. [40]	Present	Das [39]
0.00	0.3	0.4607	0.4607	0.4607	0.4607	0.4607
0.04		0.5135	0.5134	0.5134	0.5115	0.5114
0.08		0.5695	0.5698	0.5698	0.5656	0.5655
0.12		0.6304	0.6303	0.6303	0.6234	0.6233
0.14	0.0	0.6622	0.6622	0.6622	0.6536	0.6537
0.05		0.5272	0.5271	0.5271	0.5271	0.5271
		0.5	—	—	—	—
		1.5	—	—	—	—
	2.5	0.5271	0.5271	0.5271	0.5272	0.5271

TABLE 5: Result comparison for  $-Sh_x$ .

$\gamma_c \downarrow t \rightarrow$	$-Sh_x$					
	0.3	0.5	0.7	0.3	0.5	0.7
		Present		Hussain et al. [17]		
0.2	0.535254	0.438632	0.389005	0.54907	0.44765	0.38638
2	0.849652	0.815633	0.767225	0.85729	0.820922	0.78156
5	1.2252	1.16674	1.14632	1.24260	1.16967	1.143922

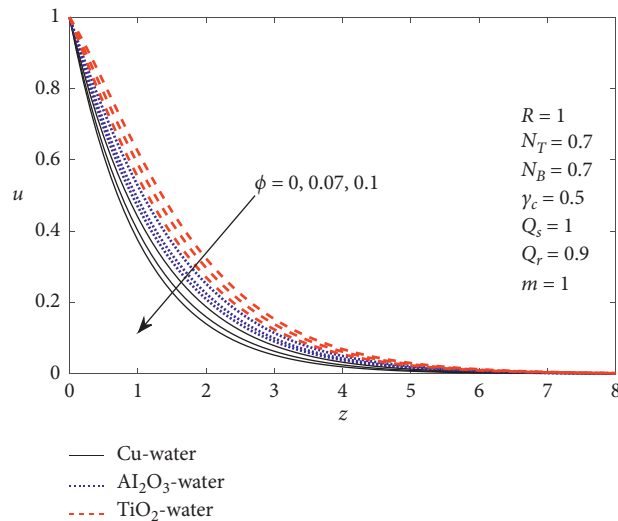


FIGURE 2: The effect of volume fraction of nanoparticles on the velocity profile.



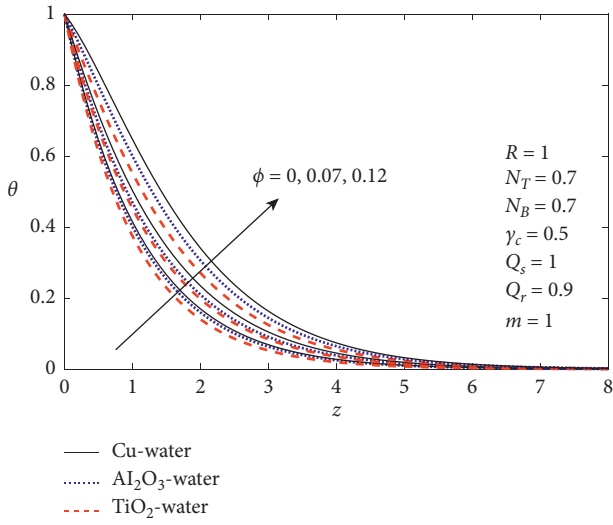


FIGURE 3: The effect of volume fraction nanoparticle on the temperature profile.

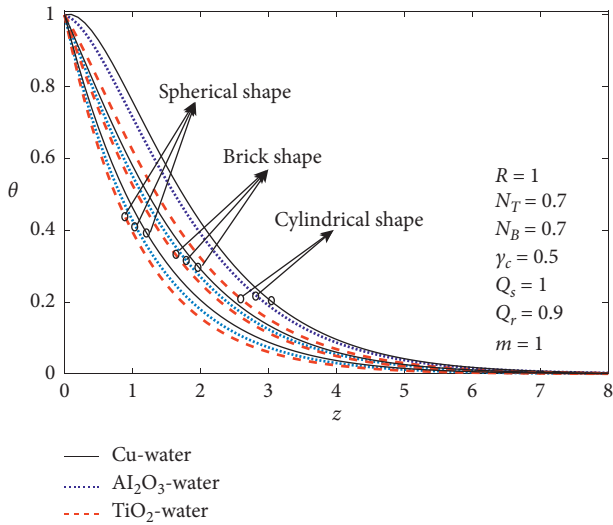


FIGURE 4: The effect of nanoparticle shape on the temperature profile.

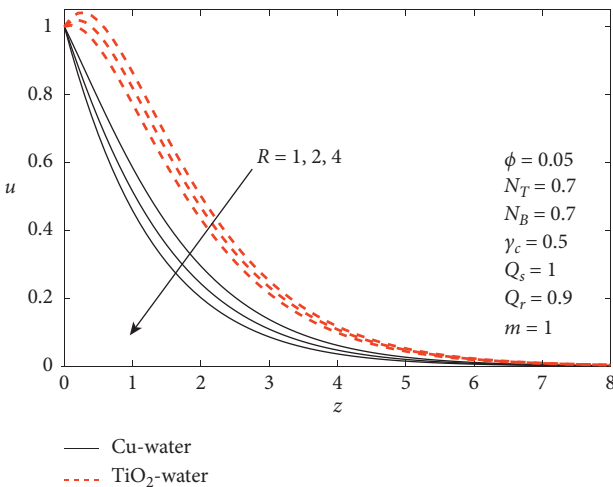


FIGURE 5: The effect of rotation parameter on the velocity profile.

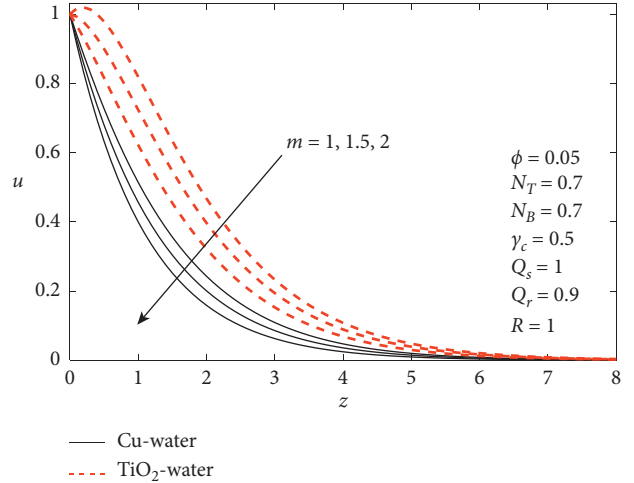


FIGURE 6: The effect of Hall current on the velocity profile.

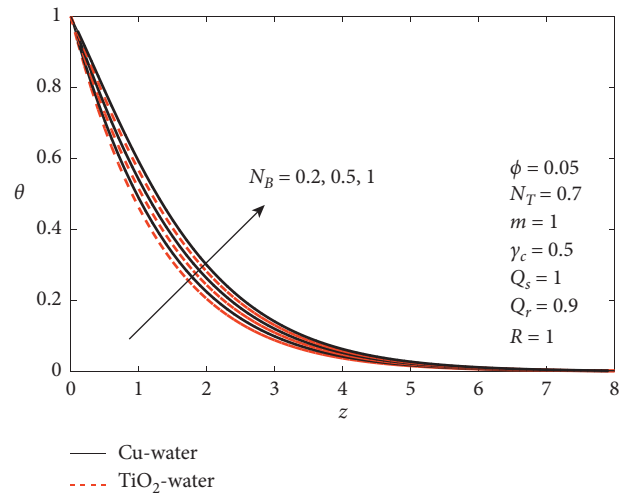


FIGURE 7: The effect of Brownian motion parameter on the temperature profile.

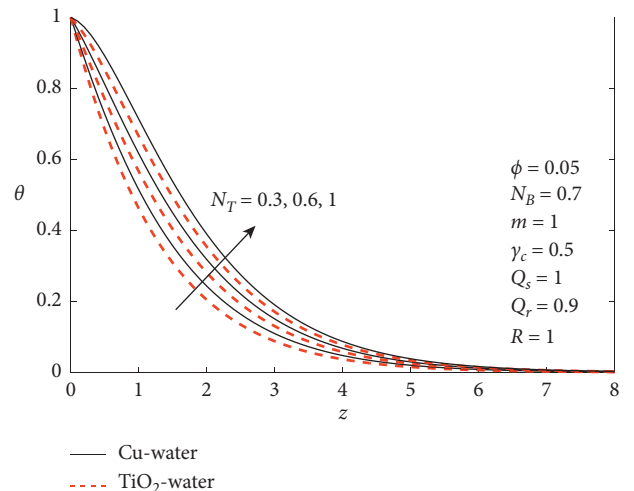


FIGURE 8: The effect of thermophoresis parameter on the temperature profile.

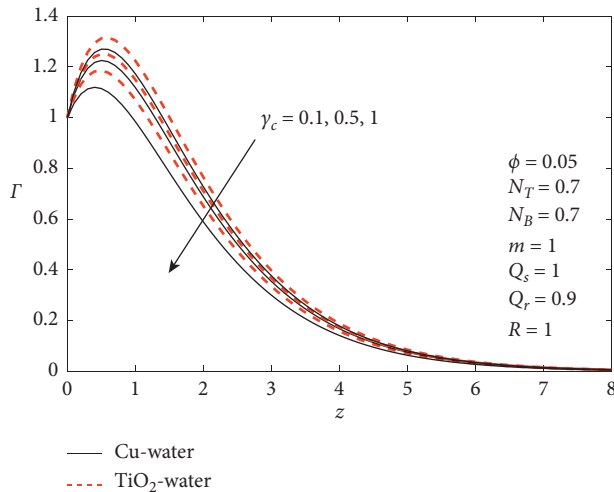


FIGURE 9: The effect of chemical reaction parameter on the concentration profile.

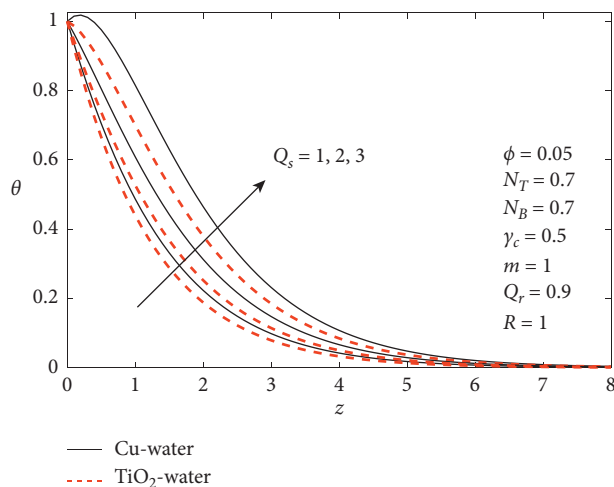


FIGURE 10: The effect of heat source parameter on the temperature profile.

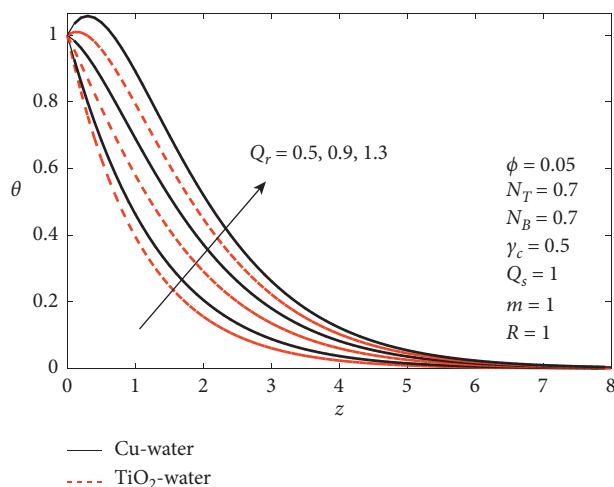


FIGURE 11: The effect of radiation parameter on the temperature profile.

and  $\text{TiO}_2$  – water nanofluid. It is clear that increase in nanoparticle volume fraction parameter  $\phi$  decreases the fluid velocity, but the temperature profiles increase. It is due to the fact that nanofluid density increases with increasing the volume fraction of nanoparticles, and it causes to slow down the nanofluid flow velocity and increases the thickness of the thermal boundary layer which improves thermal conductivity and increases surface heat transfer rate. Also, it is observed that nanofluid Cu – water heat transfer rate is greater than  $\text{Al}_2\text{O}_3$  and  $\text{TiO}_2$  rates. So, nanoparticles having high thermal conductivity enhance heat transfer more than the particles having low thermal conductivity. On the contrary, it is seen from Tables 2 and 3 that wall skin friction coefficient  $C_f$  and the Nusselt number  $\text{Nu}/\text{Re}_x$  increase with increasing in nanoparticle volume fraction for both Cu – water and  $\text{Al}_2\text{O}_3$  – water.

The influence of the nanoparticle shape on the temperature distribution of nanofluid is studied through Figure 4. This figure indicates that the heat transfer rate is higher for the cylindrical nanoparticle shape than the spherical and brick nanoparticle shapes for either Cu – water,  $\text{Al}_2\text{O}_3$  – water, and  $\text{TiO}_2$  – water nanofluid. Therefore, the spherical nanoparticle shape tends to drag more heat from the boundary layer because it has a greater surface area, while this effect is less evident for other nanoparticle shapes. Thus, the use of the cylindrical nanoparticle shape has better improvement in effective thermal conductivity when compared with other nanoparticle shapes (spherical and brick).

The influence of rotation parameter  $R$  on the velocity profiles against  $z$  is displayed in Figure 5. It observed that an increase in rotation parameter leads to decreasing the boundary layer momentum, so it decreases the values of nanofluid velocity. From Tables 2 and 3, it can be noted that the wall skin friction coefficient  $C_f$  increases with an increase in the rotation parameter, but the Nusselt number  $\text{Nu}/\text{Re}_x$  remains unchanged with both Cu – water and  $\text{Al}_2\text{O}_3$  – water.

Figure 6 presents the influence of Hall current parameter  $m$  on main velocity  $u$ . It is clear that the velocity distribution of nanofluid reduces with an increase in Hall current parameter. This happens naturally due to the fact that when the magnetic field is strengthened, it enhances the opposing force which is represented by the well-known Lorentz force.

Figures 7 and 8 show the Brownian and thermophoresis effects on the temperature profile  $\theta$ . It is seen that the temperature distribution increases with increasing for these parameters. This is due to the fact that the thermophoretic and Brownian parameters assist to improve the thermal boundary layer thickness. Also, it is observed that the heat transfer rate of Cu – water nanofluid is greater than  $\text{TiO}_2$  – water.

Figure 9 depicts the influence of chemical parameter  $\gamma_c$  on the concentration profile  $\Gamma$ . It is noticed that the increase in concentration profile is accompanied by a decrease in the chemical parameter. On the contrary, it is seen from Table 4 that the Sherwood number  $-\text{Sh}_x$  increases due to increasing the chemical parameter, but the Sherwood number decreases while increasing the time  $t$ . This implies that the chemical

reaction has tendency to increase the mass transfer rate at the surface plate, and it is reduced with the progress of time.

Figures 10 and 11 present the heat source parameter  $Q_s$  and thermal radiation parameter  $Q_r$  effects on the temperature profiles. It is clear from Figure 10 that, with an increase in the heat generation parameter, the boundary layer temperature decreases and as a consequence to decrease the thermal boundary layer thickness. In addition, it is clear from Figure 11 that, with an increase in the thermal radiation, the temperature profiles of the nanofluid increase. It is well known that the increase in the radiation parameter enhances the energy transport inside the fluid and as a consequence to increase the heat transfer rate.

## 6. Conclusion

An analysis is done to solve the magnetohydro dynamics unsteady nanofluid flow through the porous medium past a moving plate in a rotating frame with considering the heat and mass transfer. Three different types of the nanoparticles, namely, copper, aluminium oxide, and titanium dioxide, and water used as a base nanofluid are considered with various shapes (spherical, cylindrical, and brick). The important effects of nanoparticle shape, Brownian and thermophoresis diffusion, thermal radiation, ohmic and viscous dissipations have been included. Homotopy perturbation method is applied to solve the governing nonlinear partial differential equations. The efficiency of the methodology has been validated through comparison with the previously published results and observed a very close agreement. It is found that

The main velocity component decreases with increase of nanoparticle volume fraction. On the contrary, thermal properties increase with increase in nanoparticle volume fraction

The enhancement of heat transfer rate and mechanical property improvement is high in copper as compared with both aluminium oxide and titanium dioxide

Thermal conductivity of cylindrical-shaped nanoparticles is more efficient and possesses better improvement on heat transfer rate than the other shaped ones

Increase in the Brownian and thermophoresis parameter is accompanied by an increase in the thermal boundary layer thickness

Increasing Hall current and rotation parameters decreases the main fluid velocity component

HPM has a close agreement and is recommended for many nonlinear problems

## Data Availability

The data used to support the findings of this study are included within the article.

## Conflicts of Interest

The authors declare that there are no conflicts of interest regarding the publication of this paper.

## References

- [1] T. Hayat, R. Sajjad, A. Alsaedi, T. Muhammad, and R. Ellahi, "On squeezed flow of couple stress nanofluid between two parallel plates," *Results in Physics*, vol. 7, pp. 553–561, 2017.
- [2] S. U. S. Choi, "Enhancing thermal conductivity of fluids with nanoparticles," in *Proceedings of the ASME International Mechanical Engineering Congress and Exposition*, pp. 99–105, San Francisco, CA, USA, 1995.
- [3] J. A. Eastman, S. U. S. Choi, S. Li, W. Yu, and L. J. Thompson, "Anomalously increased effective thermal conductivities of ethylene glycol-based nanofluids containing copper nanoparticles," *Applied Physics Letters*, vol. 78, no. 6, pp. 718–720, 2001.
- [4] A. J. Chamkha, S. Abbasbandy, A. M. Rashad, and K. Vajravelu, "Radiation effects on mixed convection about a cone embedded in a porous medium filled with a nanofluid," *Meccanica*, vol. 48, no. 2, pp. 275–285, 2013.
- [5] M. Sheikholeslami, M. M. Rashidi, T. Hayat, and D. D. Ganji, "Free convection of magnetic nanofluid considering MFD viscosity effect," *Journal of Molecular Liquids*, vol. 218, pp. 393–399, 2016.
- [6] W. Abbas and E. A. Sayed, "Hall current and joule heating effects on free convection flow of a nanofluid over a vertical cone in presence of thermal radiation," *Thermal Science*, vol. 21, pp. 2603–2614, 2017.
- [7] B. Mahanthesh, B. Gireesha, I. Animasaun, T. Muhammad, and N. Shashikumar, "MHD flow of SWCNT and MWCNT nanoliquids past a rotating stretchable disk with thermal and exponential space dependent heat source," *Physica Scripta*, vol. 94, no. 8, Article ID 085214, 2019.
- [8] I. L. Animasaun, O. K. Koriko, K. S. Adegbe et al., "Comparative analysis between 36 nm and 47 nm alumina-water nanofluid flows in the presence of Hall effect," *Journal of Thermal Analysis and Calorimetry*, vol. 135, no. 2, pp. 873–886, 2019.
- [9] I. Ullah, S. Shafie, I. Khan, and K. L. Hsiao, "Brownian diffusion and thermophoresis mechanisms in Casson fluid over a moving wedge," *Results in Physics*, vol. 9, pp. 183–194, 2018.
- [10] P. B. S. Kumar, B. J. Gireesha, R. S. R. Gorla, and B. Mahanthesh, "Magnetohydrodynamic flow of Williamson nanofluid due to an exponentially stretching surface in the presence of thermal radiation and chemical reaction," *Journal of Nanofluids*, vol. 6, no. 2, pp. 264–272, 2017.
- [11] X. Zhou, Y. Jiang, X. Li et al., "Numerical investigation of heat transfer enhancement and entropy generation of natural convection in a cavity containing nano liquid-metal fluid," *International Communications in Heat and Mass Transfer*, vol. 106, pp. 46–54, 2019.
- [12] N. Shehzad, A. Zeeshan, R. Ellahi, and K. Vafai, "Convective heat transfer of nanofluid in a wavy channel: Buongiorno's mathematical model," *Journal of Molecular Liquids*, vol. 222, pp. 446–455, 2016.
- [13] B. Shen, L. Zheng, C. Zhang, and X. Zhang, "Bioconvection heat transfer of a nanofluid over a stretching sheet with velocity slip and temperature jump," *Thermal Science*, vol. 21, no. 6, pp. 2347–2356, 2017.
- [14] S. Jahan, H. Sakidin, R. Nazar, and I. Pop, "Analysis of heat transfer in nanofluid past a convectively heated permeable stretching/shrinking sheet with regression and stability analyses," *Results in Physics*, vol. 10, pp. 395–405, 2018.
- [15] M. A. A. Hamad and I. Pop, "Unsteady MHD free convection flow past a vertical permeable flat plate in a rotating frame of reference with constant heat source in a nanofluid," *Heat and Mass Transfer*, vol. 47, no. 12, pp. 1517–1524, 2011.

- [16] M. Sheikholeslami and D. D. Ganji, "Three dimensional heat and mass transfer in a rotating system using nanofluid," *Powder Technology*, vol. 253, pp. 789–796, 2014.
- [17] S. M. Hussain, J. Jain, G. S. Seth, and M. M. Rashidi, "Free convective heat transfer with Hall effects, heat absorption and chemical reaction over an accelerated moving plate in a rotating system," *Journal of Magnetism and Magnetic Materials*, vol. 422, pp. 112–123, 2017.
- [18] X. Zhou, Y. Jiang, Y. Hou, and M. Du, "Thermocapillary convection instability in annular two-layer system under various gravity levels," *Microgravity Science and Technology*, vol. 31, no. 5, pp. 641–648, 2019.
- [19] Y. Jiang and X. Zhou, "Heat transfer and entropy generation analysis of nanofluids thermocapillary convection around a bubble in a cavity," *International Communications in Heat and Mass Transfer*, vol. 105, pp. 37–45, 2019.
- [20] Y. Jiang, X. Zhou, and Y. Wang, "Effects of nanoparticle shapes on heat and mass transfer of nanofluid thermocapillary convection around a gas bubble," *Microgravity Science and Technology*, pp. 1–11, 2019, In press.
- [21] Y. Jiang, X. Zhou, and Y. Wang, "Comprehensive heat transfer performance analysis of nanofluid mixed forced and thermocapillary convection around a gas bubble in mini-channel," *International Communications in Heat and Mass Transfer*, vol. 110, Article ID 104386, 2020.
- [22] B. Mahanthesh, B. J. Gireesha, R. S. R. Gorla, F. M. Abbasi, and S. A. Shehzad, "Numerical solutions for magnetohydrodynamic flow of nanofluid over a bidirectional non-linear stretching surface with prescribed surface heat flux boundary," *Journal of Magnetism and Magnetic Materials*, vol. 417, pp. 189–196, 2016.
- [23] B. Mahanthesh, B. J. Gireesha, and I. L. Animasaun, "Exploration of non-linear thermal radiation and suspended nanoparticles effects on mixed convection boundary layer flow of nanoliquids on a melting vertical surface," *Journal of Nanofluids*, vol. 7, no. 5, pp. 833–843, 2018.
- [24] P. S. Kumar, B. Mahanthesh, B. Gireesha, and S. Shehzad, "Quadratic convective flow of radiated nano-jeffrey liquid subject to multiple convective conditions and Cattaneo-Christov double diffusion," *Applied Mathematics and Mechanics*, vol. 39, no. 9, pp. 1311–1326, 2018.
- [25] J. Raza, F. Mebarek-Oudina, and A. Chamkha, "Magnetohydrodynamic flow of molybdenum disulfide nanofluid in a channel with shape effects," *Multidiscipline Modeling in Materials and Structures*, vol. 15, no. 4, pp. 737–757, 2019.
- [26] T. Hayat, B. Ahmed, F. M. Abbasi, and A. Alsaedi, "Hydromagnetic peristalsis of water based nanofluids with temperature dependent viscosity: a comparative study," *Journal of Molecular Liquids*, vol. 234, pp. 324–329, 2017.
- [27] H. F. Oztop and E. Abu-Nada, "Numerical study of natural convection in partially heated rectangular enclosures filled with nanofluids," *International Journal of Heat and Fluid Flow*, vol. 29, no. 5, pp. 1326–1336, 2008.
- [28] M. A. El Kot and W. Abbas, "Numerical technique of blood flow through catheterized arteries with overlapping stenosis," *Computer Methods in Biomechanics and Biomedical Engineering*, vol. 20, no. 1, pp. 45–58, 2017.
- [29] H. A. Attia, W. Abbas, A. El-Din Abdin, and M. A. M. Abdeen, "Effects of ion slip and Hall current on unsteady Couette flow of a dusty fluid through porous media with heat transfer," *High Temperature*, vol. 53, no. 6, pp. 891–898, 2015.
- [30] H. A. Attia, W. Abbas, and M. A. M. Abdeen, "Ion slip effect on unsteady Couette flow of a dusty fluid in the presence of uniform suction and injection with heat transfer," *Journal of the Brazilian Society of Mechanical Sciences and Engineering*, vol. 38, no. 8, pp. 2381–2391, 2016.
- [31] H. A. Attia, W. Abbas, M. A. M. Abdeen, and A. A. M. Said, "Heat transfer between two parallel porous plates for Couette flow under pressure gradient and Hall current," *Sadhana*, vol. 40, no. 1, pp. 183–197, 2015.
- [32] M. Sheikholeslami, A. Shafee, M. Ramzan, and Z. Li, "Investigation of Lorentz forces and radiation impacts on nanofluid treatment in a porous semi annulus via Darcy law," *Journal of Molecular Liquids*, vol. 272, pp. 8–14, 2018.
- [33] P. S. Kumar, B. Gireesha, B. Mahanthesh, and A. J. Chamkha, "Thermal analysis of nanofluid flow containing gyrotactic microorganisms in bioconvection and second-order slip with convective condition," *Journal of Thermal Analysis and Calorimetry*, vol. 136, no. 5, pp. 1947–1957, 2019.
- [34] B. Mahanthesh, F. Mabood, B. Gireesha, and R. Gorla, "Effects of chemical reaction and partial slip on the three-dimensional flow of a nanofluid impinging on an exponentially stretching surface," *The European Physical Journal Plus*, vol. 132, no. 3, p. 113, 2017.
- [35] B. J. Gireesha, R. S. R. Gorla, and B. Mahanthesh, "Effect of suspended nanoparticles on three-dimensional mhd flow, heat and mass transfer of radiating eyring-powell fluid over a stretching sheet," *Journal of Nanofluids*, vol. 4, no. 4, pp. 474–484, 2015.
- [36] J.-H. He, "Homotopy perturbation technique," *Computer Methods in Applied Mechanics and Engineering*, vol. 178, no. 3-4, pp. 257–262, 1999.
- [37] J.-H. He, "A coupling method of a homotopy technique and a perturbation technique for non-linear problems," *International Journal of Non-Linear Mechanics*, vol. 35, no. 1, pp. 37–43, 2000.
- [38] Y. Wu and J.-H. He, "Homotopy perturbation method for nonlinear oscillators with coordinate-dependent mass," *Results in Physics*, vol. 10, pp. 270–271, 2018.
- [39] K. Das, "Flow and heat transfer characteristics of nanofluids in a rotating frame," *Alexandria Engineering Journal*, vol. 53, no. 3, pp. 757–766, 2014.
- [40] J. V. R. Reddy, V. Sugunamma, N. Sandeep, and C. Sulochana, "Influence of chemical reaction, radiation and rotation on MHD nanofluid flow past a permeable flat plate in porous medium," *Journal of the Nigerian Mathematical Society*, vol. 35, no. 1, pp. 48–65, 2016.